Improved multi-stage cross-flow fluidized bed classifier

Chameera K. Jayarathna[1,2], Michael Balfe[3], Britt M.E. Moldestad[1] and Lars-Andre Tokheim[1]
[1] *Faculty of Technology, Natural Sciences and Maritime Sciences, University of South-Eastern Norway*
[2] *SINTEF Tel-Tek, SINTEF Industry, Porsgrunn, Norway*
[3] *Turbomachinery & Process Solutions, Baker Hughes, a GE Company, Germany*

Abstract

In the present work, improvements to a novel fluidized bed solids classification system previously published by Jayarathna et al. are discussed [1]. The system is designed for a high temperature application, namely solids classification in a CO_2 capture plant incorporated with a coal-fired power plant. The capture plant is proposed to be equipped with the latest calcium looping technology, fully integrated calcium looping (FICaL). The classifier will be fed with a mixture of sorbent and heat transfer (inert) particles in the real plant at the operating temperature in between 910 °C and 600 °C. Due to the higher temperature it is not possible to use any sensitive process equipment such as filters or metal screens or any mechanically moving parts. Stepwise development of a such a system is explained in the previous publication by the authors [1]. In this work, the system is down-scaled into a smaller cold flow system, and zirconia and steel particles are used to mimic the sorbent and heat transfer solids particles in the hot flow system, respectively. Experiments and CFD simulations are carried out for the cold flow classification system. The previous fluidized bed design [1] reached an efficiency of 90% and 99% recovery (10% and 1% loss) of the lighter (zirconia) and heavier (steel) components, respectively, but a 10% loss of sorbent particles in the real system would not be economical. The new modified system reached recovery efficiencies of 97% and 98% (3% zirconia loss and 2% steel loss) of the lighter and heavier component, respectively. CFD is used as a supporting tool in the design process, and also in making improvements to the design. Improvements are made by modifying the classifier geometry such as shape, height and internal design features. The experimental results from the improved classifier are compared with the CFD predictions made by the commercially available CFD software Barracuda® 17.1. Discrepancies between the experimental and simulated results are discussed, and the Barracuda CFD model is recommended as a good simulation tool for such studies and for upscaling the simulations for the hot flow system. The improved solid classifier design obtained good enough classification performances to proceed with upscaling and continue to make further improvements in the hot flow system. The iterative design and modeling effort from this research work has produced a functional, high-efficiency classification concept that can be used for the 1000 µm HT-solids particles and the 175 µm sorbent particles in the full-scale hot-flow system.

1. Introduction

The present work is dedicated to further development of a novel particle classification system designed for second generation calcium looping technology known as ‘’Fully integrated Calcium Looping’’ (FiCaL). The specialty of the system is the low energy penalty compared to the first generation calcium looping process [2, 3] as the heat supplied in the calciner is provided indirectly through an inert solid heated in the combustion section of the coal-fired power plant. Hence, the oxyfuel burner and the air separation unit typically applied in a first generation calcium looping plant is not required in the FiCaL system.

There are several ongoing research projects related to the second generation CaL technology,

and the focus is how to provide the calcination heat indirectly in an efficient way. At the University of Darmstadt they have investigated the use of heat pipes to transfer the heat [4-6], and in the Leilac project, the concept is to provide heat by wall conduction driven by external fuel burners [7].

The use of in inert solid to provide the heat, as in the current research work, is an alternative to using heat pipes or wall conduction. Due to the particle-to-particle contact, the heat transfer area will be high, and a homogeneous temperature distribution in the system is likely due to efficient mixing sorbent and inert solids. However, the particle mixing requires subsequent separation of sorbent and inert solids, hence an efficient classifier must be developed. This is the focus of the current paper. Further information of the FiCaL process and the development of the novel cross-flow classification system is given in other papers published by the authors [1-3, 8-13].

The classification of particle mixtures into pure particle streams is sometimes required in powder handling industries. Different classification techniques can be applied, including gravitational classifiers, cascade classifiers, inertial classifiers, centrifugal classifiers, and fluidized bed classifiers [14].

In fluidized bed classification, a stream of gas is used to separate particulate solids into different fractions according to particle size or other particle characteristics, such as density or shape. Depending on the design of the classifier, forces including gravity, aerodynamic drag, centrifugal force, and collision force act on the particles during classification [15]. Fluidized bed classifiers operate on the gravitational-counter flow separation principle. The residence time of the particle mixture in this technique may facilitate separation.

In a typical fluidized bed classifier, the gas velocity is set higher than the terminal velocity of the fine fraction. The fine particles are carried out of the unit by the gas stream, while the coarse particles are concentrated at the bottom of the unit. Fluidized bed classifiers are generally used for the separation of binary particle mixtures. The quality of the separation is given as the recovery of the fine fraction in the top product and the coarse fraction in the bottom product. In order to enhance the separation performance, classifiers are often equipped with collision surfaces [15].

This work represents a continuation of the development of the novel high-temperature solids classifier previously described by the authors [1-3, 8-13]. The classifier is meant for separation of sorbent (calcium oxide) particles and inert (alumina) heat transfer particles in a CO_2 capture plant, and this represents a second-generation calcium looping system. Under normal operating conditions, the classification is conducted at approximately 910 °C, which is the required calcination temperature in a CO_2 rich environment. The classifier was designed to satisfy the following criteria:

- High degree of particle separation (to minimize the sorbent makeup requirement)
- No moving parts (to avoid operational problems, in particular considering the high temperature in a hot-flow system)
- Low pressure drop, low maintenance requirements, and simple operation (to minimize operational costs)
- Not overly complex geometry (to avoid difficult construction and maintenance)

The performance of the classifier concept was tested using a cold-flow lab-scale classifier system [1] and was also studied by means of CFD simulations [9]. Due to downscaling from hot-flow to cold-flow (ambient temperature and pressure) conditions, applying Glicksman

scaling rules [16-18], zirconia and steel particles were used in place of calcium oxide and alumina particles, respectively. Furthermore, air was used as the fluidization medium in place of CO_2. The system achieved 90 % and 99 % recovery of the lighter (zirconia) and heavier (steel) particles, respectively. While the inert solids loss of 1% was acceptable, a 10% loss of sorbent particles is not economically viable, as it would require using of an excessively high fraction of the sorbent makeup. Based on these results, modification of the novel solids classifier was deemed to be necessary to improve its classification efficiency and thereby reduce the losses.

Based on the experience gained with the previously described cold-flow lab-scale system, and aided by CFD simulations, several improvements to the previous classifier geometry [1, 9, 11] were implemented in a new version of the classifier. A modified unit was constructed, and new experiments were performed in the lab. Simulations of the new classifier were also carried out using the CFD software Barracuda (version 17.1).

The purpose of the current work is to report the significant improvements that have been achieved using this modified cross-flow fluidized bed classifier. Theoretical considerations and results from both lab-scale experiments and CFD simulations of the improved system are included.

2. Experimental setup

Selected characteristics of the particles and gases used in the hot-flow and cold-flow systems are given in Table 1, and additional characteristics of the particles used in the cold-flow experiments are given in Table 2.

The experimental setup is shown in Figure 1. Zirconia and steel particles were fed into the classifier via screw conveyors, a mixer, a hopper, and a rotary valve. Pressurized air for fluidization was blown in from the bottom of the unit, and entered the classifier via five compartments, each equipped with a mass flow controller. One tank was used to collect the coarse particles from the bottom exit, while another tank collected the fine particles from the top exit after separation in a cyclone. A bag filter was used to collect the particles not captured in the cyclone. The static pressure was measured at 15 different positions, three in each compartment. A more detailed theoretical analysis of this classifier system has been presented in a previous paper [1], and hence is not repeated here.

All the experiments were done at atmospheric conditions, and both solids flow rate and air flow rate were varied. Further information regarding the experiments are shown in section 4. The main measurement in the experiments was the amounts of mass collected in the top and bottom bins. 10 parallels were run at the beginning to understand the behavior and the repeatability of the experiments. It was found that the standard deviation of the results from each case was very low. It was concluded that running three parallels of each case would be sufficient, and this gave a standard deviation lower than 0.003kg.

Table 1: Particle and gas characteristics for the hot-flow and cold-flow systems

	Hot-flow system			Optimum cold-flow system			Actual cold-flow system used in the experiments		
	Gas	Sorbent	HT solids	Gas	Sorbent	HT solids	Gas	Sorbent	HT solids
Material	CO_2	Lime-stone	Alu-mina	Air	-	-	Air	Zirconia	Steel
Size [µm]	-	175	1000		50	284	-	69	290
Density [kg/m³]	0.45	1760	3000	1.21	4682	7981	1.21	3800	7800
Operating temperature [°C]	910	910	910	20	20	20	20	20	20
Operating pressure [Pa]	101325	101325	101325	101325	101325	101325	101325	101325	101325
Viscosity [Pa·s] x 10^7	443.8	-	-	181.6	-	-	181.6	-	-

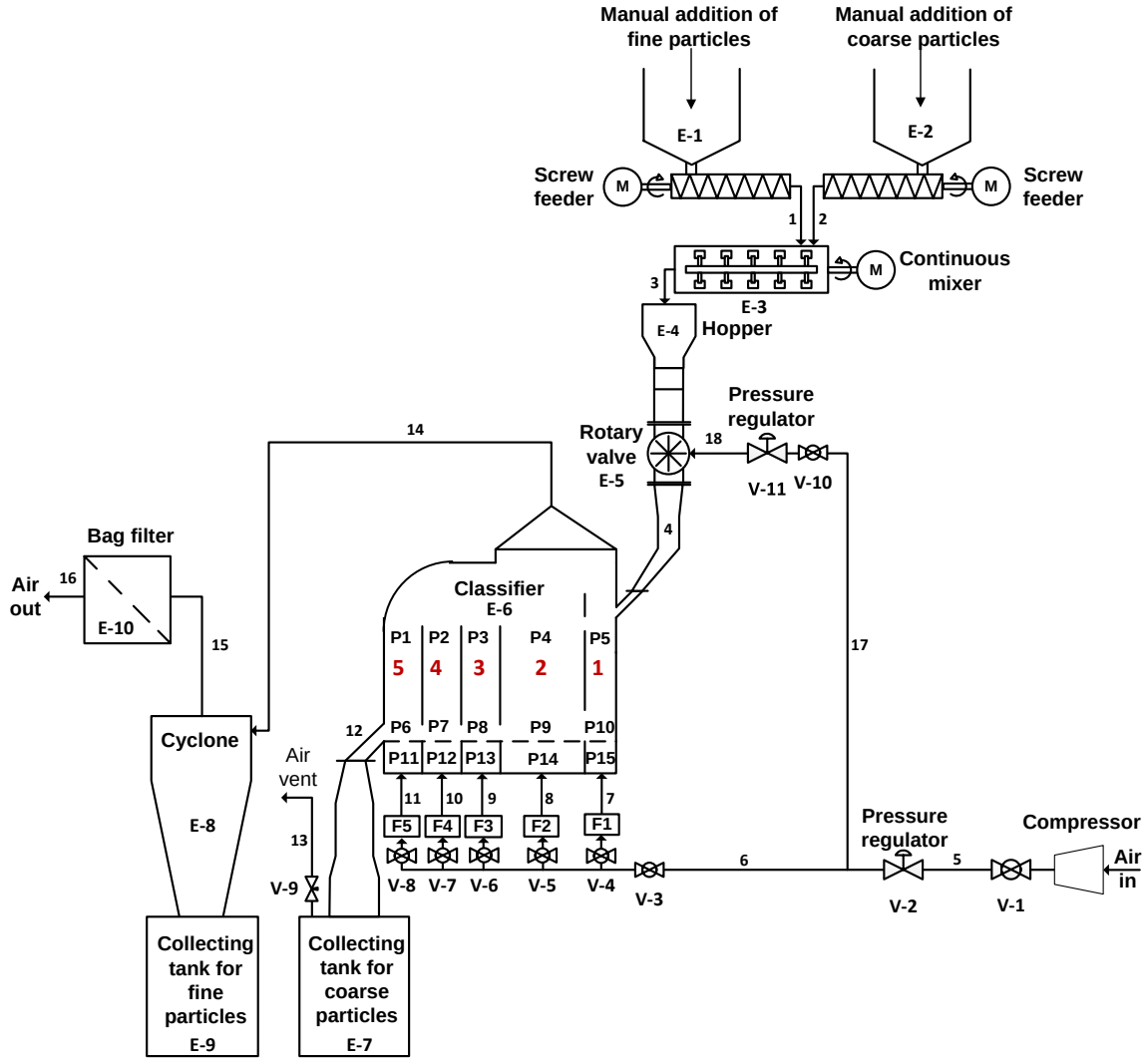

Figure 1: Process instrumentation diagram of the lab-scale classifier system

The installed classifier, which was built in transparent Lexan plastic to facilitate visual observation of the system, is shown in Figure 2. The new experiments were carried out using the same procedures as those applied in the previous system [1].

Table 2: Particle characteristics

Property	**Zirconia**	**Steel**
Skeletal density	3830 kg/m³	7790 kg/m³
Bulk density	2270 kg/m³	4500 kg/m³
Bulk to skeletal density ratio	0.6	0.6
Particle diameter	45-100 µm	230-350 µm
Median particle size	69 µm	290 µm
Commercial name	Microblast	Amasteel shot
Composition	ZrO_2: 60-70%, SiO_2: 28-33%, Al_2O_3: <10%	Fe: >96%, C: <1.2%, Mn: <1.3%, Si: <1.2%, Cr: <0.25%
Terminal settling velocity in air at 1 atm and 293 K	0.27 m/s	3.95 m/s

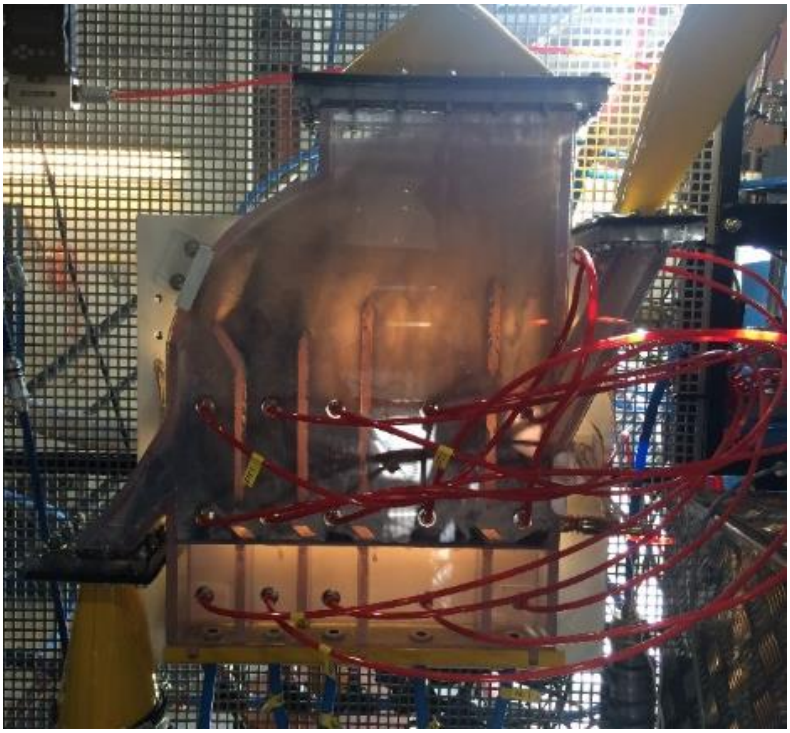

Figure 2: Photograph of the classifier unit showing the air inlets, solids inlet, gas/fine particles outlet, coarse solids outlet, and pressure taps

3. Modifications to the cross-flow fluidized bed classifier

The previous and new classifier designs are shown in Figure 3. The five modifications implemented in the new version of the classifier are indicated as A, B, C, D and E in Figure 3(b). Each of these modifications is described and explained below.

The left side of the upper horizontal wall in the classifier has been changed (A). The left compartment mainly contains heavier particles but may also contain a small portion of lighter particles. In the previous design, the lighter particles tended to bounce back from the horizontal top wall and return to the bottom of the compartment, putting them at risk of being lost via the bottom exit. The new smooth and curved geometry facilitates the entrainment of the fine particles and thereby reduces the loss.

The top section of the leftmost vertical baffle has been tilted (B). The air velocity in compartment 5 (see Figure 1) is higher than in the other compartments. Due to the high

velocity, there is a possibility for the heavy particles to be removed from the dense phase, become entrained by the fluidization gas, and exit the classifier via the top outlet. This in turn would reduce the classification efficiency. By tilting the baffle wall, most of the heavier particles are prevented from leaving the compartment, as they will be rebounded after hitting the tilted section.

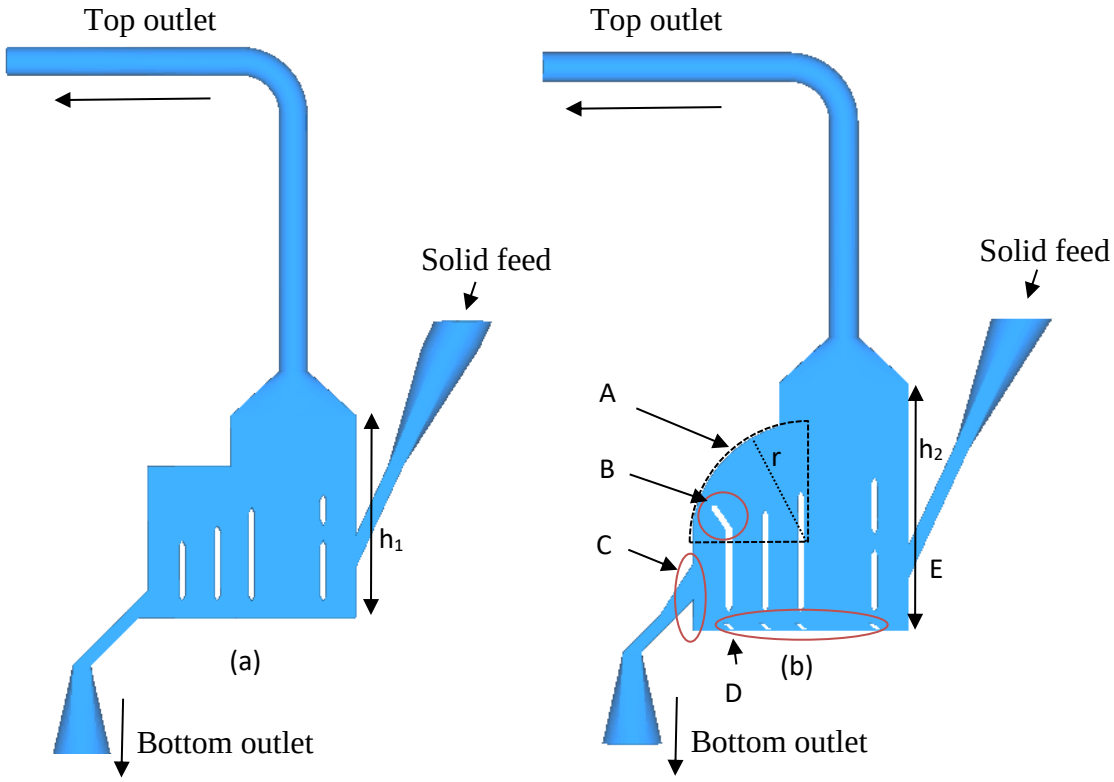

Figure 3: Earlier design of the cross-flow fluidized bed (a), and the updated version (b). The modifications are indicated by the letters A-E

The particle-laden gas flow exiting through the space between the curved wall and the tip of the tilted baffle is quite different from the flow in the other compartments. The velocity of the flow is higher due to the reduced cross section. Due to this increased velocity and the curved shape of the wall, the particles are affected by centrifugal forces. The heavier particles tend to concentrate along the curved wall, and due to their higher angular velocity, most shoot out horizontally at the end of the curved wall and move towards the right-hand wall of the classifier. (Visual observations during experiments have confirmed that these particles return to the first compartment and are mixed into the dense particle bed.) The lighter particles leaving the curved wall have less momentum, and will become entrained by the vertical gas stream and exit via the top outlet. The combined effect of modifications A and B should improve the classification efficiency in this area. A sketch of the flow pattern resulting from modifications A and B is shown in Figure 4.

Modification C involved elevation of the bottom particle outlet, and enlargement of the cross section of this outlet. The resulting outlet weir will increase the particle residence time in the classifier, and will effectively reduce the horizontal particle momentum. As the particles must change direction from horizontal to vertical to exit via the bottom outlet, the lighter particles in the dense bed will have a higher possibility of becoming entrained by the gas. In addition, the cross-sectional area of the bottom outlet has been increased, facilitating the flow of heavier particles into the bottom outlet without unnecessary resistance. The weir height and the outlet

cross section were chosen based on CFD simulations of different elevations and cross sections. The combination that resulted in the highest simulated classification efficiency was chosen.

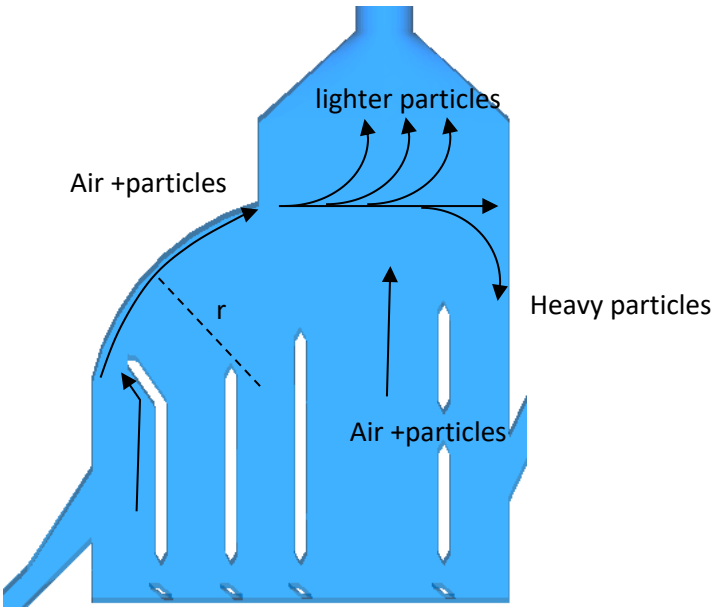

Figure 4: Expected flow pattern of particles resulting from modifications A and B

Additionally, inclined baffles were installed at the bottom of the bed (modification D). In fast fluidization, the particles in the freeboard either rise or return to the dense bed depending their size and density [19]. If the particles entering the unit could be directed into the freeboard in a more efficient way, this would increase the classification efficiency. Particles tend to move to the freeboard along with gas bubbles [19], but thin layers of lighter particles can become trapped at the bottom of the dense phase. To avoid this, small baffles with a 45° inclination were placed close to the air distributor plate below the walls of each of the compartments. The bottom layer of the dense particle bed, which moves horizontally away from the feeding point is then forced to change direction and to some extent "jump" into the middle area of each compartment as the air bubbles rise out of the dense bed. This may provide more opportunities for the particles to enter the freeboard area. The particle movement resulting from this modification is illustrated in Figure 5.

In general, the entrainment of particles in the freeboard region of a fluidized bed decreases with height until the transport disengaging height (TDH) is reached. Above the TDH, the entrainment rate of the particles does not change significantly [15]. Information about the TDH in an entrainment fluidized bed is explained by Kunii and Levenspiel [15]. The TDH calculation for the previous version of the classifier is shown in a previous publication [1].

The TDH is an important parameter that is used to optimize the freeboard height of a gas-particle fluidized bed in order to minimize particle loss. The solids thrown up to the freeboard contain the whole spectrum of particles in the mixture, but the larger and heavier particles fall back to the bed, whereas the smaller and lighter particles are carried out. Thus, a taller freeboard promotes particle classification with an accurate air flowrate. However, above the TDH, the freeboard has no return flow. This means that a freeboard higher than the TDH increases classification efficiency. Based on visual observations, it was speculated that the height of the freeboard in the earlier design of the classifier did not reach the TDH, and therefore, the height has been increased from h_1 to h_2 in the latest version (see Figure 3, E). However, the design of the internal compartment walls was not changed. This was because gas bubbles are forced

to burst at the end of the internal compartment walls, and short compartment walls help to maintain a lower dense particle bed and a higher freeboard area, which should improve the classification efficiency.

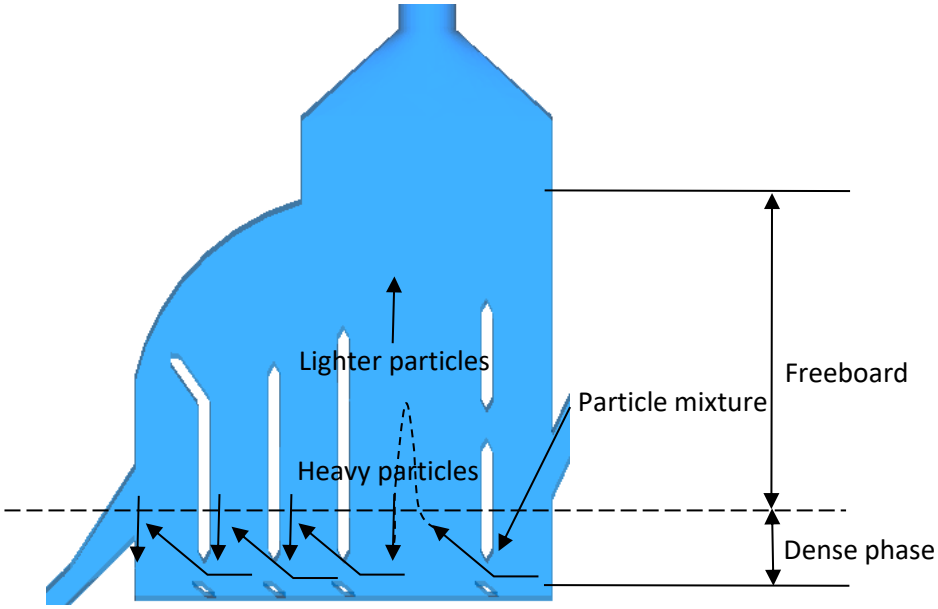

Figure 5: Expected particle flow pattern resulting from the installation of inclined baffles at the bottom of the classifier (modification D)

4. Case definitions

Experiments were carried with the modified lab-rig to determine the extent to which its classification efficiency would be improved. A selection of cases run in the previous rig was repeated with the modified geometry to allow direct comparison of the results. The solids feed rate, fluidization air flow rate, and feed composition were varied as shown in Table 3. The superficial air velocities in the compartments are listed in Table 4.

Table 3: Experimental cases

Zirconia (wt%)	Steel (wt%)	Air flow rate [Nm³/h]	Solids loading [kg/kg] for both geometries
0	100	82	8-57
28	72	40	15
		82	7 and 14
		136	5
100	0	82	4-26

Table 4: Superficial air velocities in compartment 1-5 at three different air flow rates

Air flow rate [Nm³/h]	1	2	3	4	5
82	1.1	1.0	1.4	1.9	2.0
136	1.9	1.1	1.7	2.3	5.8
40	0.5	0.5	0.7	0.9	0.9

5. CFD model description

In Barracuda, the gas phase is calculated by solving the Navier-Stokes equations, and a Lagrangian description combined with the MP-PIC method is used for the particle phase [20-22]. The gas and particle phases are coupled via an interphase drag model. The governing equations have been described in detail in a recent publication by the authors [9] and are therefore not repeated here. However, the drag model applied in the CFD simulations is described below.

5.1. Drag model

The drag model calculates the force F_p acting on a given particle, and is given by:

$$F_p = m_p D(u_g - u_p) \tag{1}$$

The Wen-Yu model [23, 24] was one of the drag models used in the present study. The drag function and the drag coefficient used in this model are given by:

$$D = \frac{3}{8} C_d \frac{\rho_g |u_g - u_p|}{\rho_p r_p} \tag{2}$$

$$C_d = \begin{cases} \frac{24}{Re}\theta_g^{n_0} & Re < 0.5 \\ \frac{24}{Re}\theta_g^{n_0}(c_0 + c_1 Re^{n_1}) & 0.5 \le Re \le 1000 \\ c_2 \theta_g^{n_0} & Re > 1000 \end{cases} \tag{3}$$

The constants have the following values: $c_0 = 1.0$, $c_1 = 0.15$, $c_2 = 0.44$, $n_0 = -2.65$ and $n_1 = 0.687$.

The Reynolds number is calculated as:

$$Re = \frac{2\rho_g r_p |u_g - u_p|}{\mu_g} \tag{4}$$

The Ergun drag model [25, 26] was also used in the present study. In this model, the drag function is given by:

$$D = 0.5\left(\frac{c_1 \theta_p}{\theta_g Re} + c_0\right)\frac{\rho_g |u_g - u_p|}{\rho_p r_p} \tag{5}$$

Here, $c_0 = 2$ and $c_1 = 180$.

The values recommended by Pitault et al. [27] for c_0 and c_1 are 1.75 and 150, respectively, but in Barracuda the default values are 2 and 180. In the present work, which was based on the study performed by Jayarathna et al. [11], the c_1 value was reduced to 47 for zirconia

particles, while the Barracuda default value (180) was used for steel particles.

The Wen-Yu model is suitable for more dilute systems [23] and the Ergun model [25] is suitable at higher packing fractions [28]. The Wen-Yu/Ergun model combines the two models, and is therefore valid over a wider particle concentration range. The drag coefficient is then calculated as:

$$D = \begin{cases} D_1 & \theta_p < 0.75\theta_{CP} \\ (D_2 - D_1)\left(\dfrac{\theta_p - 0.75\theta_{CP}}{0.85\theta_{CP} - 0.75\theta_{CP}}\right) & 0.75\theta_{CP} \geq \theta_p \geq 0.85\theta_{CP} \\ D_2 & \theta_p > 0.85\theta_{CP} \end{cases} \quad (6)$$

Here D_1 is the Wen-Yu drag function defined in equation (3) and D_2 is the Ergun drag function defined in equation (5).

5.2. Computational model, mesh and geometry

The geometry of the model is shown in Figure 6. In Barracuda, a cut cell meshing technique is used to model complex geometries with a cartesian grid [29], and a relatively high number of cells is required to provide sufficient resolution of the geometry details. A detailed view of the grid for the solids classifier is shown in Figure 6(a). The grid was generated with 102168 cells. The boundary types are shown in Figure 6(b). Transient points to monitor the pressure drop in the simulated classifier were defined at the same locations as in the real geometry, as shown in Figure 6(b).

Experiments were carried out at a temperature of approximately 20 °C and atmospheric pressure, and the simulations were run using the same conditions. Additionally, for the particle to particle interaction, a close pack volume fraction of 0.6 was used and the maximum momentum redirection from a collision was set to 40%. The normal to wall momentum retention, tangent to wall momentum retention, and diffuse bounce values were set to 0.3, 0.99, and 2 respectively. These parameters are important for the particle to wall interactions.

The sphericity of the particles was set to 0.8 based on the report of Chladek et al.[13]. The time step was set to 0.001 s, and each simulation was run until a pseudo steady state was reached (typically less than 40 s), i.e., when the accumulated mass in the system became constant (an example is shown in Figure 10).

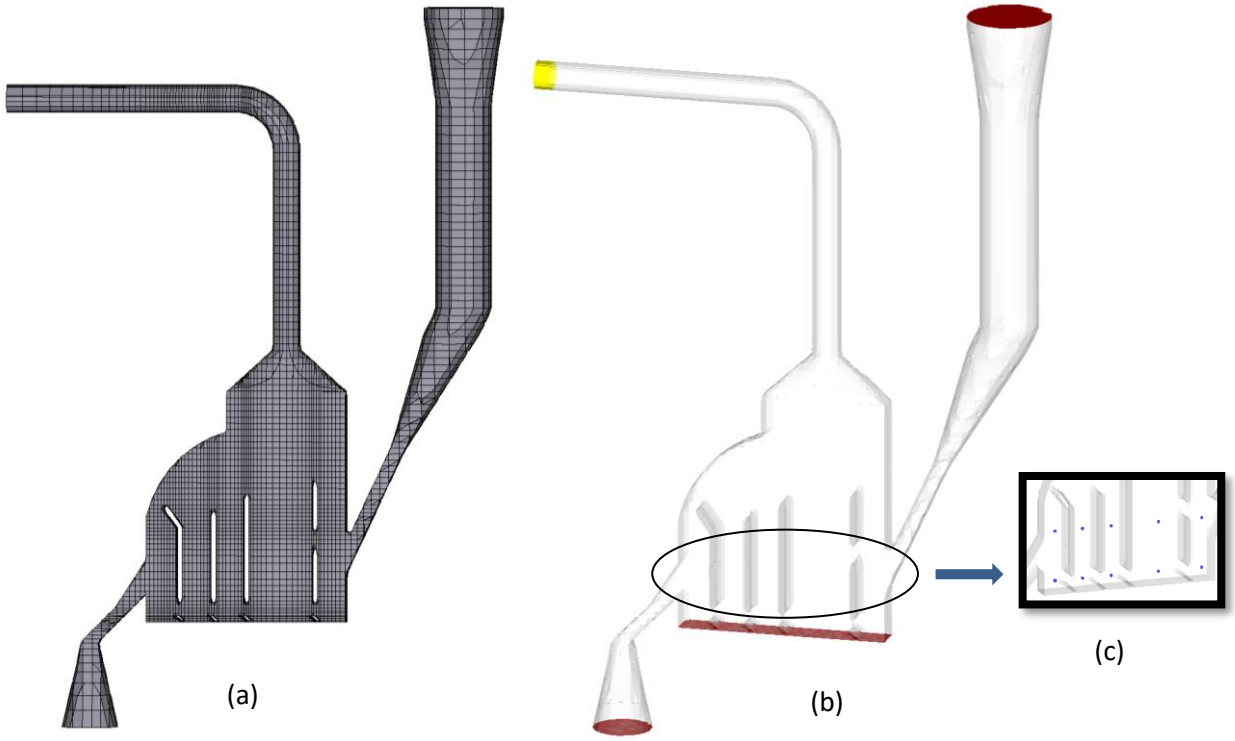

Figure 6: (a) Grid for the CFD simulations, (b) boundary types (yellow: pressure boundary, red: flow boundary), and (c) pressure monitoring points

6. Results and discussion

The modified geometry (referred to as 5.1v) described in Section 2 was used on the cases defined in Section 4. As described above, the experiments included cases with pure solids as well as mixtures of particles.

6.1. Experiments with pure particles

Feeding pure zirconia and pure steel into the classifier provides information about how each of the particle types (light/small or heavy/coarse) behaves in the classifier unit, and gives an indication of how the classifier modifications impact the classification efficiency. Such information will be useful when interpreting the behavior of the particle mixtures.

As described by Jayarathna et al. [1], the main classification principal under fluidization conditions is the separation of particles based on differences in their terminal settling velocities. The fluidization air velocity is increased from compartment 1 to 5 to increase the classification efficiency. The selected velocities used as the reference air velocities in each compartment were 1.1, 1, 1.4, 1.9, and 2 m/s for compartments 1 to 5, respectively (see Table 4). All the velocities were intermediate between the calculated terminal velocities of the zirconia (0.27 m/s) and steel (3.95 m/s) particles. Thus, the zirconia particles are likely to become entrained by the air and exit via the top outlet, whereas the steel particles are likely to remain in the bed and exit via the bottom outlet.

With the previous geometry (referred to as 3.0v), it was difficult to route all the zirconia particles to the top outlet when only zirconia particles were fed into the system, even when the gas velocity was significantly higher than the single particle settling velocity [1]. The capability of the previous classifier to carry zirconia particles out via the top exit was also diminished with increased solids loading in the classifier. Figure 7 shows that the modified geometry significantly improved the classification of pure zirconia particles. The bottom exit loss dropped by approximately 20 wt% for all cases. This is likely due to the modifications A, D, and E described in Section 2. The classifier still did not discharge all the zirconia particles via the top outlet, but the loss was reduced to 3% at a solid loading of 4 kg/kg, and extrapolation of the data suggests that the zirconia bottom exit loss would be close to 0% at a solid loading of 2 kg/kg.

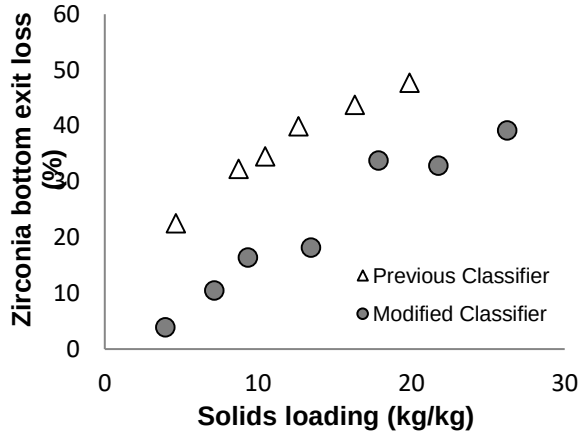

Figure 7: Zirconia loss via the bottom outlet during classification of a pure zirconia particle feed (total air flow rate: 82 Nm³/h)

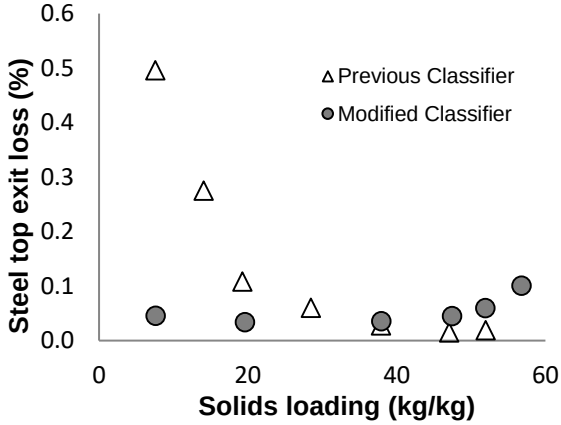

Figure 8: Steel loss via the top outlet during classification of a pure steel particle feed (total air flow rate: 82 Nm³/h)

Almost all the steel particles leave through the bottom exit, as would be expected from the theoretical calculations of particle settling velocity (Figure 8). This was also the case in the previous classifier, although the steel loss was slightly reduced in the modified classifier at low solids loadings. For example, the steel loss was approximately 0.5 wt% at a solid loading of 8 kg/kg, but the modified geometry exhibited a steel loss to 0.05 wt% under the same conditions. The key modifications responsible for this improvement are most likely modifications B, C, and E, as described in Section 3.

6.2. Experiments with particle mixtures

Figure 9 summarizes the selected classification experiments. The experiment names in Figure 9 reflect the solids loading and fluidization air flow rate used. In the following discussion, each of the experiments is assigned a number from 1 (highest S/G value) to 4 (lowest S/G value).

In Experiment 1, the air flow rate (40 Nm³/h) was lower than the reference air flow rate, and the steel loss was 0%. However, the zirconia loss via the bottom outlet in this case was very high (50-60%), resulting in very poor classification. Experiment 4, in which a high air flow rate (136 Nm³/h) was applied, resulted in low zirconia loss in the previous classifier (about 6%), and extremely low zirconia loss in the modified unit (about 0.8%). However, the loss of steel particles was unacceptably high (30-60%). Experiments 2 and 3 resulted in less extreme loss values than experiments 1 and 4. Experiment 3 in particular resulted in the best tradeoff

between the loss of zirconia (3% in the modified geometry, 9% in the previous geometry) and loss of steel (2% vs 1%). Experiment 2 resulted in higher zirconia loss than Experiment 3 for both geometries. This was due to the higher solids loading applied in Experiment 2, as the fluidization air flow rates were the same.

As explained in section 3, the bubbles created at the dense bed area carry particles to the top of the dense bed and then release the particles into the freeboard by blasting. The vertical baffles in the modified classification chamber convert bubbles into slugs and force them to blast at the top end of the baffles. The particles released at the freeboard are allowed to follow the airflow and leave the classifier or return back to the dense bed, depending on the air flow rate and the terminal velocity of the particles. Experimental case 1 (from Figure 9) has a relatively low air flow rate, and the air bubbles that blast at the bottom of the freeboard have too little energy to release more particles into the free board area. Furthermore, the particles released into the freeboard have less air to create a significant drag on the particles to carry bigger and heavier particles out of the classifier. As a result of that, a higher fraction of smaller and lighter zirconia particles ends up in the bottom product. Exactly the opposite happened in case 4; air bubbles (slugs) with more energy due to the higher air flow rate released more particles into the freeboard area and a higher air flow carried more particles out of the classifier, including a larger fraction of heavy steel particles. The optimum is laying in between these two cases. Case 3 is found to be close to the optimum, but there is still room for further fine tuning of the classification system.

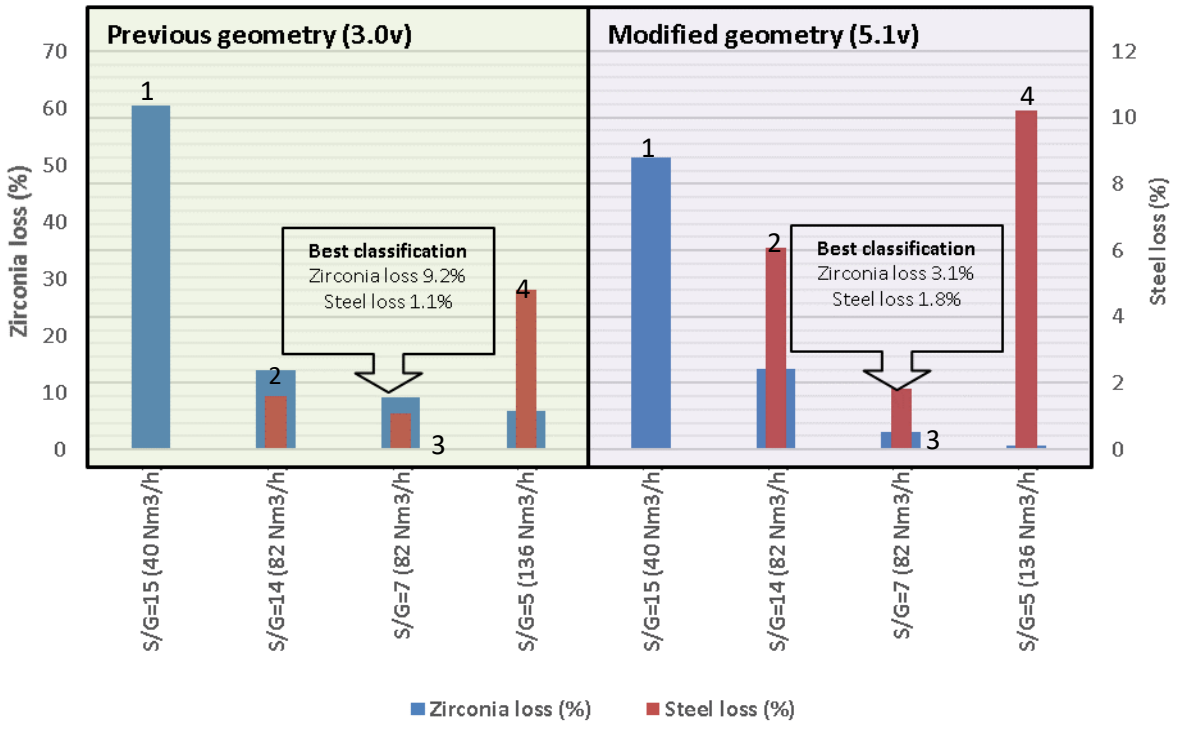

Figure 9: Zirconia bottom exit loss and steel top exit loss at different solids loading values and air flow rates using a constant feed mixture (28 wt% zirconia and 72 wt% steel)

6.3. Experimental observations vs CFD predictions

Only the simulation results for Experiment 3 are discussed here, as this experiment resulted in the best classification performance for both the 3.0v geometry and the 5.1v geometry.

According to Figure 10, the accumulated particle mass inside the classifier reached a stabilized, pseudo steady state after approximately 40 s.

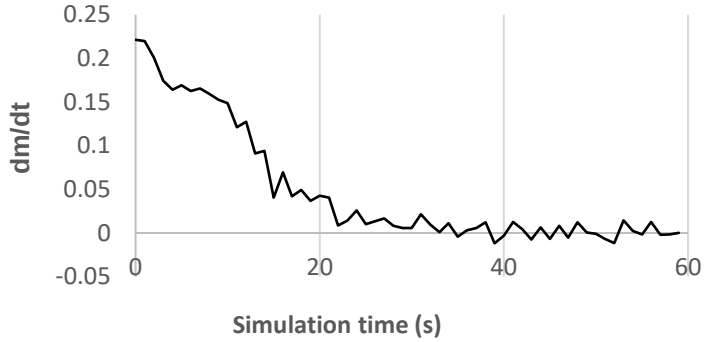

Figure 10: Change in the accumulated mass inside the classifier for Experiment 3 run in the modified geometry (5.1v)

Figure 11 (a) shows the flow pattern in the simulated geometry (5.1v). The steel and zirconia particles are represented by red and blue, respectively. The figure shows a clear classification of the particle mixture into red (steel) and blue (zirconia) particles. As indicated in Figure 11 (b), both the simulation and the experiment indicated that most of the zirconia particles were removed from the dense bed from the first three compartments, as counted from the right-hand side of the classifier. Relatively similar flow patterns were observed, and the flow occurred as described in section 3. However, the accumulated particle mass in each compartment appeared to be slightly higher in the CFD simulations than in the lab system. This was supported by the averaged pressure drop data, shown in Figure 12.

Once the classifier has reached the pseudo steady state, the averaged pressure drop in each compartment represents the accumulated particle mass in the compartment. Both the CFD simulations and the experiments showed very low pressure drops for the 3.0v geometry. This was due to the absence of the outlet weir for the heavy particles in this geometry, which resulted in the particles leaving the classifier much faster than in the 5.1v geometry; the residence time of the particles was much shorter. The elevated bottom particle outlet of the 5.1v geometry resulted in much higher bubbling fluidized bed being formed behind the weir.

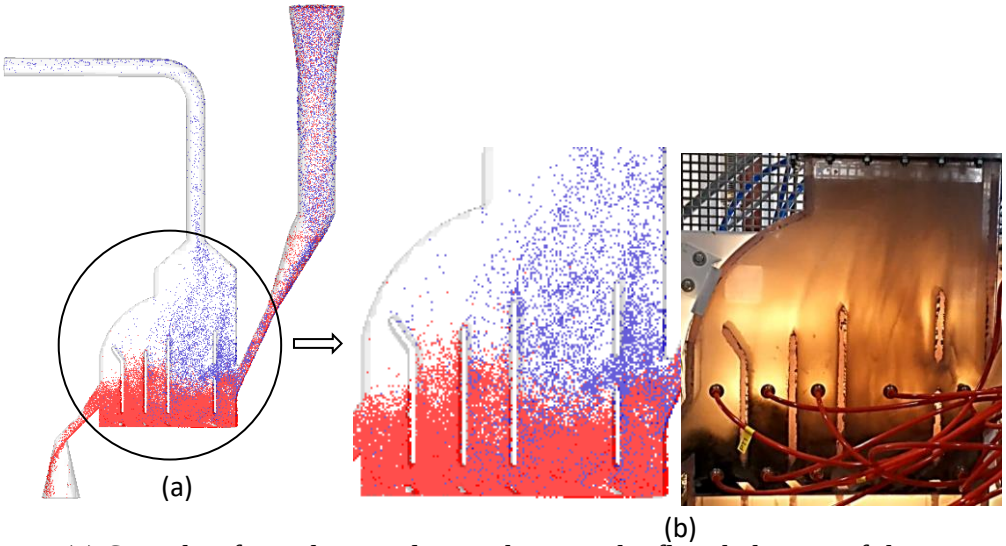

Figure 11: (a) Snapshot from the simulation showing the flow behavior of the two particle types (red: steel, blue: zirconia) (b) Simulation vs experimental results

The pressure drop graph indicated some deviation between the simulations and experiments for the 5.1v geometry. This may have been due to over-prediction of particle accumulation in the simulated classifier.

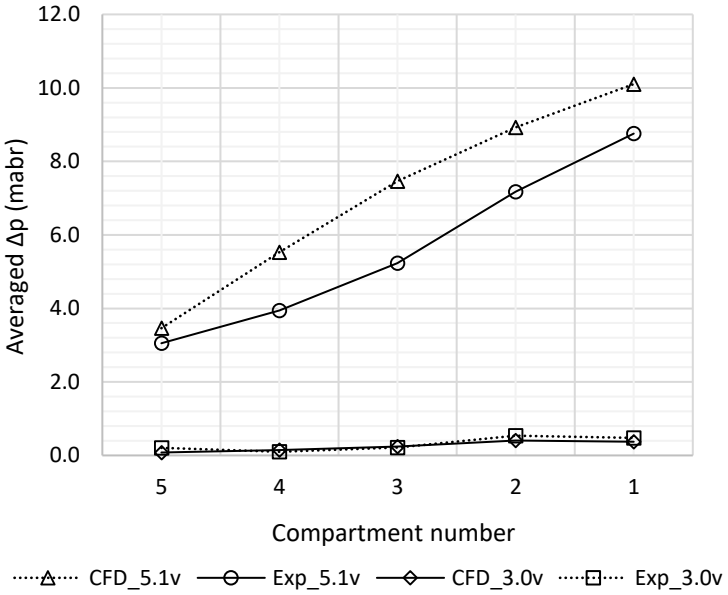

Figure 12: Simulated (CFD) and measured (experimental) pressure drops in each compartment (data averaged at the pseudo steady state) for the previous (3.0v) and modified geometry (5.1v)

Table 5 presents the experimentally observed classification efficiency and the Barracuda predicted values for the 5.1v geometry for Experiment no.3. In general, both the experimental and CFD predicted values were low, but considerable deviation was observed between the results. The main reason for the discrepancy could be the slugging effect from the rotary valve in the lab-rig; the feed rate pulsations caused by the cells in the rotary valve are not captured in the simulations. This slugging effect in the experiments caused solids loading values to temporarily increase above the average value (7 kg/kg). As has been observed in both simulations and lab-scale experiments, higher solids loadings result in poorer classification efficiency. With a non-pulsing feed rate, lower losses of zirconia would likely have been measured..

Table 5: Particle losses observed in the experimental tests and simulations with Barracuda for the modified geometry (5.1v) for Experiment 3

Particle type	**Zirconia**	**Steel**
Experiments	3.1	1.8
CFD simulations	0.1	0.6

7. Conclusions

Experiments and Barracuda simulations demonstrated that the modified geometry described in this report represents a significant improvement over the previous geometry in terms of classification efficiency. The results indicated that the classifier was able to achieve a sorbent bottom exit loss of approximately 1-3% while maintaining the steel top exit loss at a low level of 1-2%.

The Barracuda simulations provided accurate predictions, and were able to qualitatively capture the particle flow pattern in the classifier. Barracuda proved to be a good tool, both for process unit design and for interpretation of the experimental results.

When operating the cold-flow lab-rig with a sorbent bottom exit loss of 3.1%, the steel top exit loss was 1.8%, both of which can be considered low. Hence, it can be concluded that the iterative design and modeling effort from this research work has produced a functional, high-efficiency classification concept that can be used for the 1000 µm HT-solids particles and the 175 µm sorbent particles in the full-scale hot-flow system.

Acknowledgements

The authors would like to thank research assistants Mahesh Ediriweera, Amila Chandra, Thanushan Abeywickrama, Janith Bandara, Widuramina Samindranath, Sumudu Karunarathna, and Bovinda Ahangama for their valuable assistance during the experiments. The support of chief scientist Chandana Ratnayake, scientist Tonje Thomassen, and scientist Franz Hafenbrädl at SINTEF Tel-Tek, and from chief engineer Øyvind Johansen at the University of Southeast Norway, is also highly appreciated. The financial support from Gassnova and GE is also gratefully acknowledged. The authors would also like to thank Sam Clark from CPFD Software, LLC for valuable technical support with Barracuda.

References

[1] C. K. Jayarathna, J. Chladek, M. Balfe, B. M. E. Moldestad, and L.-A. Tokheim, "Impact of solids loading and mixture composition on the classification efficiency of a novel cross-flow fluidized bed classifier," *Powder Technology,* vol. 336, pp. 30-44, 2018/08/01/ 2018.

[2] C. K. Jayarathna, A. Mathisen, L. E. Øi, and L.-A. Tokheim, "Process Simulation of Calcium Looping with Indirect Calciner Heat Transfer," presented at the SIMS 56, Linkoping, Sweden, October 7–8, 2015, 2015. Available: http://www.ep.liu.se/ecp/119/ecp15119.pdf

[3] C. K. Jayarathna, A. Mathisen, L. E. Øi, and L.-A. Tokheim, "Aspen Plus® Process Simulation of Calcium Looping with Different Indirect Calciner Heat Transfer Concepts," *Energy Procedia,* vol. 114, pp. 201-210, 7// 2017.

[4] M. Junk, M. Reitz, J. Ströhle, and B. Epple, "Thermodynamic evaluation and cold flow model testing of an indirectly heated carbonate looping process," presented at the 2nd International Conference on Chemical Looping, Darmstadt, Germany, 26-28 September, 2012.

[5] M. Junk, M. Reitz, J. Ströhle, and B. Epple, "Thermodynamic Evaluation and Cold Flow Model Testing of an Indirectly Heated Carbonate Looping Process," *Chemical Engineering & Technology,* vol. 36, no. 9, pp. 1479-1487, 2013.

[6] M. Reitz, M. Junk, J. Ströhle, and B. Epple, "Design and Erection of a 300 kWth Indirectly Heated Carbonate Looping Test Facility," *Energy Procedia,* vol. 63, pp. 2170-2177, // 2014.

[7] T. P. Hills, M. Sceats, D. Rennie, and P. Fennell, "LEILAC: Low Cost CO2 Capture for the Cement and Lime Industries," *Energy Procedia,* vol. 114, pp. 6166-6170, 2017/07/01/ 2017.

[8] C. K. Jayarathna, B. M. Halvorsen, and L.-A. Tokheim, "Experimental and Theoretical Study of Minimum Fluidization Velocity and Void Fraction of a Limestone Based CO2 Sorbent," *Energy Procedia,* vol. 63, no. 0, pp. 1432-1445, // 2014.

[9] C. K. Jayarathna, M. Balfe, B. M. E. Moldestad, and L. A. Tokheim, "Comparison of experimental results from operating a novel fluidized bed classifier with CFD simulation results applying seven different drag models," *Particuology,* vol. Submitted, 2017.

[10] C. Jayarathna, "Development of a fluidized bed particle classifier for application in calcium looping with indirect heat transfer : Experiments and simulations," 2017: 21, University College of Southeast Norway, Kongsberg, 2017.

[11] C. K. Jayarathna, B. M. E. Moldestad, and L. A. Tokheim, "Validation of results from Barracuda® CFD modelling to predict minimum fluidization velocity and pressure drop of Geldart A particles," in *SIMS 58*, Reykjavik, Iceland, 2017, vol. Conference proceedings, 2017.
[12] W. S. Amarasinghe, C. K. Jayarathna, B. S. Ahangama, B. M. E. Moldestad, and L.-A. Tokheim, "Experimental study and CFD modelling of fluidization velocity for Geldart A, B and D particles," *International Journal of Modeling and Optimization,* vol. 7, no. 3, 2017.
[13] J. Chladek, C. K. Jayarathna, B. M. E. Moldestad, and L.-A. Tokheim, "Fluidized bed classification of particles of different size and density," *Chemical Engineering Science,* vol. 177, pp. 151-162, 2018/02/23/ 2018.
[14] M. Shapiro and V. Galperin, "Air classification of solid particles: a review," *Chemical Engineering and Processing: Process Intensification,* vol. 44, no. 2, pp. 279-285, 2// 2005.
[15] F. N. C. I.V. Klumpar, T.A. Ring,, "Air Classifiers," *Chemical Engineering,* March, 1986.
[16] L. R. Glicksman, "Scaling relationships for fluidized beds," *Chemical Engineering Science,* vol. 39, no. 9, pp. 1373-1379, 1984/01/01 1984.
[17] L. R. Glicksman, "Scaling relationships for fluidized beds," *Chemical Engineering Science,* vol. 43, no. 6, pp. 1419-1421, 1988/01/01 1988.
[18] L. R. Glicksman, M. Hyre, and K. Woloshun, "Simplified scaling relationships for fluidized beds," *Powder Technology,* vol. 77, no. 2, pp. 177-199, 1993/11/01 1993.
[19] D. L. O. Kunii, *Fluidization engineering*. Boston,Mass.: Butterworths, 1991.
[20] D. M. Snider, "An Incompressible Three-Dimensional Multiphase Particle-in-Cell Model for Dense Particle Flows," *Journal of Computational Physics,* vol. 170, no. 2, pp. 523-549, 7/1/ 2001.
[21] P. J. O'Rourke, P. Zhao, and D. Snider, "A model for collisional exchange in gas/liquid/solid fluidized beds," *Chemical Engineering Science,* vol. 64, no. 8, pp. 1784-1797, 4/15/ 2009.
[22] M. J. Andrews and P. J. O'Rourke, "The multiphase particle-in-cell (MP-PIC) method for dense particulate flows," *International Journal of Multiphase Flow,* vol. 22, no. 2, pp. 379-402, 1996/04/01 1996.
[23] C. Y. Y. Wen, Y.U., "Mechanics of fluidization," *Chemical Engineering Progress Symposium,* pp. 100-111, 1966.
[24] M. K. Patel, K. Pericleous, and M. Cross, "Numerical Modelling of Circulating Fluidized Beds," *International Journal of Computational Fluid Dynamics,* vol. 1, no. 2, pp. 161-176, 1993/01/01 1993.
[25] S. Ergun, "Fluid flow through packed columns," *Chemical Engineering Progress,* vol. 48, p. 89, 1952.
[26] R. Beetstra, M. A. van der Hoef, and J. A. M. Kuipers, "Drag force of intermediate Reynolds number flow past mono- and bidisperse arrays of spheres," *AIChE Journal,* vol. 53, no. 2, pp. 489-501, 2007.
[27] I. Pitault, D. Nevicato, M. Forissier, and J.-R. Bernard, "Kinetic model based on a molecular description for catalytic cracking of vacuum gas oil," *Chemical Engineering Science,* vol. 49, no. 24, pp. 4249-4262, 1994/01/01 1994.
[28] D. Gidaspow, *Multiphase Flow and Fluidization: Continuum and kinetic theory description*. 24-28 Oval Road, London: Academic Press, Inc., 1993.
[29] E. M. Ryan *et al.*, "Multi-phase CFD modeling of solid sorbent carbon capture system," *Powder Technology,* vol. 242, no. 0, pp. 117-134, 7// 2013.